Computer Modeling in
Engineering & Sciences

Tech Science Press

DOI: 10.32604/cmes.2022.017914

ARTICLE

Numerical Simulation of Reiner–Rivlin Nanofluid Flow under the Influence of Thermal Radiation and Activation Energy over a Rotating Disk

Arfan Shahzad[1,2], Muhammad Imran[1,*], Muhammad Nawaz Naeem[1] and Mohsan Raza[1]

[1]Department of Mathematics, Government College University Faisalabad, Faisalabad, 38000, Pakistan

[2]Department of Sciences & Humanities, National University of Computer and Emerging Sciences, Chiniot-Faisalabad Campus, Faisalabad, 38000, Pakistan

[*]Corresponding Author: Muhammad Imran. Email: drmimranchaudhry@gmail.com

Received: 16 June 2021 Accepted: 23 November 2021

ABSTRACT

In current study, the numerical computations of Reiner–Rivlin nanofluid flow through a rotational disk under the influence of thermal radiation and Arrhenius activation energy is considered. For innovative physical situations, the motile microorganisms are incorporated too. The multiple slip effects are considered in the boundary conditions. The bioconvection of motile microorganism is utilized alongside nanofluids to provide stability to enhanced thermal transportation. The Bioconvection pattern in various nanoparticles accredits novel applications of biotechnology like the synthesis of biological polymers, biosensors, fuel cells, petroleum engineering, and the natural environment. By deploying some suitable similarity transformation functions, the governing partial differential equations (PDEs) of the flow problem are rehabilitated into dimensionless forms. The accomplished ordinary differential equations (ODEs) are solved numerically through the bvp4c scheme via a built-in function in computational MATLAB software. The upshots of some prominent physical and bioconvection parameters including wall slip parameters, thermophoresis parameter, Brownian motion parameter, Reiner–Revlin nanofluid parameter, Prandtl number, Peclet number, Lewis number, bioconvection Lewis number, and the mixed convection parameter against velocity, temperature, nanoparticles concentration, and density of motile microorganism profiles are dichotomized and pondered through graphs and tables. The presented computations show that the velocity profiles are de-escalated by the wall slip parameters while the thermal and solutal fields are upgraded with augmentation in thermophoresis number and wall slip parameters. The presence of thermal radiation enhances the temperature profile of nanofluid. The concentration profile of nanoparticles is boosted by intensification in activation energy. Furthermore, the increasing values of bioconvection Lewis number and Peclet number decay the motile microorganisms' field.

KEYWORDS

Reiner–Rivlin nanofluid; bioconvection; motile swimming microorganisms; rotational disk; multiple slip conditions; bvp4c

Nomenclature

B^*	Mixed convection parameter
b	Chemotaxis constant
C	Concentration of nanomaterials, $\mathrm{molL^{-1}}$
C_f	Skin friction coefficient
C_w	Concentration of nanomaterials at the surface
C_∞	Concentration of nanomaterials away from the surface
D	Microorganisms' diffusion coefficient, $\mathrm{m^2s^{-1}}$
D_B	Brownian diffusion coefficient, $\mathrm{m^2s^{-1}}$
D_m	Microorganisms' diffusivity, $\mathrm{m^2s^{-1}}$
D_T	Thermophoresis diffusion coefficient, $\mathrm{m^2s^{-1}}$
E	Activation energy parameter
E_a	Activation energy, J
g^*	gravity
j_m	Motile microorganism flux
j_w	Local mass flux, $\mathrm{Kgm^{-2}s^{-1}}$
Kr	Chemical reaction rate
k	Thermal conductivity, $\mathrm{Wm^{-1}K^{-1}}$
k^*	Mean absorption coefficient
Lb	Bioconvection Lewis number
Le	Lewis number
N	Density of microorganisms, $\mathrm{m^{-3}}$
Nb	Brownian diffusion parameter
Nt	Thermophoresis number
Nu	Local Nusselt number
N_w	Microorganism concentration at the surface
N_∞	Microorganism concentration away from the surface
Pe	Peclet number
Pr	Prandtl number
q_w	Local heat flux, W
n	Power Law index
Rb	Bioconvection Rayleigh number
Rc	Buoyancy ratio parameter
Rd	Thermal radiation parameter
r	Radius of disk, m
Sh	Local Sherwood number
Sn	Microorganisms' density number
T	Temperature of fluid, K
T_0	Reference temperature of fluid
T_w	Temperature of fluid at the surface
T_∞	Temperature of fluid away from the surface
u, v, w	Velocity components, $\mathrm{ms^{-1}}$
W_c	Maximum cell swimming speed

Greek Symbols

λ	Reiner–Rivlin fluid parameter
α_m	Thermal diffusivity, $\mathrm{m^2s^{-1}}$
β^{**}	Coefficient of thermal expansion
$\beta_1, \beta_2, \beta_3, \beta_4, \beta_5$	Wall slip parameters
γ_1	Thermal slip coefficient
γ_2	Concentration slip coefficient

γ_3	Microorganisms slip coefficient
δ	Temperature difference parameter
δ_1	Microorganism's difference parameter
σ^*	Stefan–Boltzman constant
θ	Dimensionless temperature
ϕ	Dimensionless volume fraction of nanoparticles
χ	Dimensionless microorganisms' density function
ζ	Similarity variable
ρ_f	Density of fluid, kgm^{-3}
ρ_m	Microorganism particles density
$(\rho c)_p$	Heat capacity of nanoparticles, $Jm^{-3}\ K^{-1}$
$(\rho c)_f$	Heat capacity of base fluid, $Jm^{-3}\ K^{-1}$
μ	Dynamic viscosity of nanoliquid, Nsm^{-2}
ν	Kinematic viscosity of nanoliquid, m^2s^{-1}
ω	Angular velocity

Subscript

w	Condition at the wall
0	Ambient condition
f	Fluid
∞	Condition at the free stream

1 Introduction

The flow of spinning disks is critical in both theoretical and practical considerations. In principle, such flows are among the fluid mechanics' problems that the Navier–Stokes equations may effectively solve. These flows are realistically based on the cases such as geophysics, microbiology, and other industrial implementations such as turbomachinery. Whether the vortex formed, or small eddy motion created automatically leads to the talk of rotating fluids. The flow of spinning disks is typically employed in many tracts viz., nutriment processing, chemical reactors, designing turbines, engine gearing and brake components, disk cleaners, viscometry, medical gadgetry, typical rotating geometry of internal cooling, compressors, rotors, and cyclone separator. The study of the heat transfer phenomenon in the presence of thermal radiation has also achieved great attention by scientists in recent decades. The impact of thermal radiation at high temperatures cannot be denied as it encountered a variety of interesting applications in power generation, solar energy systems, nuclear industries, missiles technology, semiconductor wafers, etc.

Non-Newtonian fluid flows are found more in research and technology than Newtonian fluids. Scientists, biologists, and mathematicians worked tirelessly to explain and grasp the rheological characteristics of non-Newtonian fluids. These fluids have difficult nature of the operation and are complicated to apply in industries owing to their changeable composition. Therefore, this work discusses the bioconvective, steady, and incompressible flow of the Reiner–Rivlin nanofluid over a rotating disk. An empirical approach using a bvp4c method is proposed for the current study. Nanofluid is classified as nanometer-sized particles suspended in normal fluids with a diameter of less than 100 nm. Nanofluids have properties that make them potentially useful in many applications of heat transfer. They exhibit enhanced thermal conductivity and the convective heat transfer coefficient compared to the base fluid. Nanofluids are useful in a variety of science and industrial applications, including biomedicine, automotive cooling, transformer cooling, electrical device cooling, heat exchanger, the development of liquid displays, and nuclear power plants [1–5]. Hafeez et al. [6] analyzed the stagnation point flow of Oldroyd-B fluid over a rotatory disk.

Hayat et al. [7] studied the influence of magnetohydrodynamics (MHD) 3-dimensional flow of nanoliquids and thermal transport of convective boundary conditions. Ellahi et al. [8] investigated slip's role in two-phase nanofluid flow. Alsaedi et al. [9] examined entropy production in MHD Eyring–Powell nanofluid flow because of viscous dissipation, nonlinear mixed convection, and Joule heating. Khan et al. [10] studied the effect of thermal and solutal transport behavior in the Maxwell flow of nanofluid on the solar radiative expansion surface. Gireesha et al. [11] created a numerical model of nonlinearly thermal radiation as well as chemical reactions on a Maxwell nanofluid layer. Heat and mass diffusion of Maxwell nanoparticles were combinedly studied by Khan et al. [12] as they traveled through a linearly stretching surface. Nadeem et al. [13] analyze numerically the heat transformation process for Maxwell nanofluids. Khan et al. [14] investigate the impact of nonlinear heat radiation with nanomaterials and Arrhenius activation energy on the flowing of a generalized 2nd-grade nanofluid. Alghamdi [15] investigated the erratic flow of carbon nanotubes-type fluids between two moveable discs. Ullah et al. [16] proposed a computational model of the Darcy–Forchheimer nanoliquids motion by a rotating disc with partial slip. Tabassum et al. [17] investigated the numerical behavior of non-Newtonian Reiner–Rivlin nanofluid partial slip and heat transportation basis on a spinning disc. Attempts [18–20] offer more detail on the Reiner–Rivlin fluid.

Bioconvection models (swimming of motile microorganisms) have a crucial role in various real life-fields including model construction, pharmaceutical manufacturing, hydrodynamics system, sedimentary waterways, micro-fluidics machines, biofuels, food processing, gas-bearing, hydrodynamics fabrication, microbial increased oil recovery, lubrication materials, polymer construction, etc. Microorganisms are used in medicines as antibiotics and help to create vaccines. Furthermore, there has been reported to be a great combination of nanoliquids and bioconvective processes. The bioconvection of motile microorganisms is utilized alongside nanofluids to provide stability to enhanced thermal transportation. Microorganism particles are used in a wide range of commercial and industrial product categories, such as ethanol, biodiesel, biofuels, microsystems, and bio-fertilizers. Ansari et al. [21] scrutinized the effects of motile swimming microorganisms and nanomaterials over the bioconvection magnetohydrodynamics (MHD) movement of Casson-type liquid at the nonlinearly stretched boundary. Rashad et al. [22] addressed the bio-convection process in nanoliquid flow by the circular cylinder. The mass movement of steady incompressible MHD liquid immediately the stagnation level with the deferral of microscopic particles under the stretchable surface is evaluated by Mamatha et al. [23]. Iqbal et al. [24] discussed the effect of motile gyrotactic microorganisms absorbed in the nanoliquid is often by control of mass flux, bio-convection, as well as energy convection. Kasaragadda et al. [25] inspected the consequence of highly hydrophobic surfaces on the acceptance of nanoparticle-reinforced biomaterial structures. Waqas et al. [26] used both cylinder and plate to observe the bioconvective flow by considering Wu's slip conditions. Amirsom et al. [27] focused on a bi-axial stretched layer for the 3-dimensional motion of gyrotactic motile microorganisms in bioconvection nanoliquids. Uddin et al. [28] studied the mathematical model of bio-nano-convection transition with blowing and multiple slips through the horizontal layer. Ferdows et al. [29] discovered the conceptual boundary layer flow of cylinder heat and mass transportation in the motile microorganism living in a viscous liquid. Khan et al. [30] examine bioconvection in two stretchable rotating disks utilizing entropy imitation. Li et al. [31] examined the behavior of a transformed second grade nanofluid with bioconvection properties in the presence of Wu's slip. Muhammad et al. [32] used slip results from a wedge to discover the cause of bioconvection in Carreau nanofluid. More research on bioconvection is being conducted [33–35]. Zhang et al. [36] examined the influence of thermal radiation on the stretching/shrinking of a disc in a bioconvective rate type nanofluid with

Arrhenius activation energy. Waqas et al. [37] examined the passage of an Oldroyd-B fluid around a spinning disk containing swimming motile microorganisms. Naqvi et al. [38] scrutinized the bioconvection flow of a few stress fluids involving nanomaterials, magnetic fields, and gyrotactic microorganisms in rotating disks.

1.1 Scope of the Study

The heat transfer in electronic devices is the main challenge in the world due to shorter sizing. To fulfill this gap nanofluids with bioconvection are more useful due to the higher thermal conductivity of nanoparticles. Therefore, in this article, we explore the bioconvection analysis of Reiner–Rivlin nanofluid flow over a rotating disk. For innovative physical situations, the consequences of motile microorganisms along with multiple slip effects are also part of this study. The bioconvection of motile microorganisms is utilized alongside nanofluids to provide stability to enhanced thermal transportation. In literature, the structure of the proposed problem under the impacts of multiple slip constraints is not discussed yet so pertinent results are given importance to fill this gap. The effects of some asymmetrical controlling parameters including wall slip parameters, thermophoresis parameter, Brownian motion parameter, Reiner–Revlin fluid parameter, Prandtl number, Peclet number, Lewis number, bioconvection Lewis number, and the mixed convection parameter on the flow, concentration, density of motile microorganism, and thermal field are examined thoroughly. The numerical outcomes are obtained by using the bvp4c method in MATLAB software. The graphical trend of different controlling parameters besides subjective flow fields is discussed and elaborated.

2 Mathematical Modeling

Consider the three-dimensional, steady, and incompressible flow of Reiner–Rivlin nanofluid containing gyrotactic motile microorganisms over a rotating disk. The rotation of nanofluid is taken about the z—axis normal to the surface with angular velocity ω, (u, v, w) the velocity components along r, ϕ, z (see Fig. 1). The flow formulation is developed by addressing the effects of thermal radiation to the energy Eq. (5) and Arrhenius activation energy to the nanoparticle's concentration Eq. (6). It is presumed that T_w, C_w, N_w and T_∞, C_∞, N_∞ are the temperature, concentration of nanoparticles, the density of motile microorganisms at the surface and far away from the surface respectively. The highly nonlinear equations of the flow problem are transformed into ordinary ones with suitable similarities. For this purpose, we employed the bvp4c scheme. The tensor of Reiner–Rivlin fluid is given by [17]:

$$\tau_{ij} = -p\delta_{ij} + \mu e_{ij} + \mu_c e_{ik} e_{kj}; e_{jj} = 0. \tag{1}$$

Here $\tau_{ij}, p, \mu_c, \delta_{ij}$ and $e_{ij} = \left(\partial u_i/\partial x_j\right) + \left(\partial u_j/\partial x_i\right)$ designate the deformation rate tensor, pressure, and stress tensor and cross-viscosity coefficient, respectively. The governing flow equations are proposed by [17,37]:

$$u_r + \frac{u}{r} + w_z = 0, \tag{2}$$

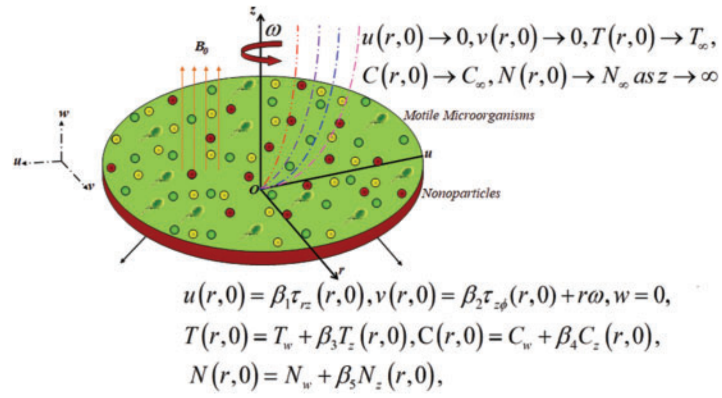

Figure 1: The geometrical shape of the problem

$$\rho\left(uu_r + wu_z + \frac{v^2}{r}\right) = \partial_r(\tau_{rr}) + \partial_r(\tau_{rz}) + \frac{\tau_{rr} - \tau_{\phi\phi}}{r}, \tag{3}$$

$$\rho\left(uu_r + wu_z + \frac{uv}{r}\right) = \frac{1}{r^2}u_r\left(r^2\tau_{r\phi}\right) + \partial_z\left(\tau_{z\phi}\right) + \frac{\tau_{r\phi} - \tau_{\phi r}}{r}$$
$$\rho(uu_r + wu_z) = \frac{1}{r^2}\partial_r(r\tau_{rz}) + \partial_z(\tau_{zz}) + \frac{1}{\rho_f}\begin{bmatrix}\left(1 - C_f\right)\rho_f\beta^{**}g^*(T - T_\infty) \\ -\left(\rho_p - \rho_f\right)g^*(C - C_\infty) \\ -(N - N_\infty)g^*\gamma\left(\rho_m - \rho_f\right)\end{bmatrix}, \tag{4}$$

$$uT_r + wT_z = \alpha_m\left(T_{rr} + \frac{1}{r}T_r + T_{zz}\right) + \frac{(\rho c)_\rho}{(\rho c)_f}\left(D_B\left(T_rC_r + T_zC_z\right)\right)$$
$$+ \frac{D_T}{T_\infty}\left((T_r)^2 + (T_z)^2\right) + \frac{1}{(\rho c)_f}\frac{16\sigma^* T_\infty^3}{3k^*}T_{zz}, \tag{5}$$

$$uC_r + wC_z = D_B\left(C_{rr} + \frac{1}{r}C_r + C_{zz}\right) + \frac{D_T}{T_\infty}\left(T_{rr} + \frac{1}{r}T_r + T_{zz}\right)$$
$$- Kr^2(C - C_\infty)\left(\frac{T}{T_\infty}\right)^n \exp\left(\frac{-E_a}{K_1 T}\right), \tag{6}$$

$$uN_r + wN_z + \frac{bW_c}{(C_w - C_\infty)}\left[\partial_z(NC_z)\right] = D_m N_{zz}, \tag{7}$$

Furthermore, distortion rate tensor's components are [17]:

$$e_{rr} = 2u_r; e_{\phi\phi} = 2\frac{u}{r}; e_{zz} = 2w_z; e_{r\phi} = e_{\phi r} = r\partial_r\left(\frac{v}{r}\right), e_{z\phi} = e_{\phi z} = v_z, e_{rz} = e_{zr} = u_z + w_r \tag{8}$$

Stress tensor components are assumed to be defined as [17]:

$$\tau_{rr} = -p + \mu(2u_r) + \mu_c\left\{4(u_r)^2 + (u_z + w_r)^2 + \left(v_r - \frac{v}{r}\right)^2\right\}, \tag{9}$$

$$\tau_{zr} = \mu\left(u_z + w_r\right) + \mu_c\left\{\left(u_z + w_r\right)\left(2u_r\right) + \left(v_z\right)\left(v_r - \frac{v}{r}\right) + \left(2w_z\right)\left(u_z + w_r\right)\right\}, \tag{10}$$

$$\tau_{\phi\phi} = -p + \mu\left(2\frac{u}{r}\right) + \mu_c\left\{4\frac{u^2}{r^2} + \left(v_z\right)^2 + \left(v_r - \frac{v}{r}\right)^2\right\}, \tag{11}$$

$$\tau_{r\phi} = \mu\left(v_r - \frac{v}{r}\right) + \mu_c\left\{\left(v_r - \frac{v}{r}\right)\left(2u_r\right) + \left(\frac{2u}{r}\right)\left(v_r - \frac{v}{r}\right) + \left(v_z\right)\left(u_z + w_r\right)\right\}, \tag{12}$$

$$\tau_{z\phi} = \mu v_z + \mu_c\left\{\left(u_z + w_r\right)\left(v_r - \frac{v}{r}\right) + 2\left(\left(v_z\right)\left(\frac{u}{r}\right) + \left(w_z\right)\left(v_z\right)\right)\right\}, \tag{13}$$

$$\tau_{zz} = -p + 2\mu\left(w_z\right) + \mu_c\left\{4\left(w_z\right)^2 + \left(v_z\right)^2 + \left(u_z + w_r\right)^2\right\}, \tag{14}$$

The physical boundary conditions are [17,37]:

$$\left.\begin{array}{l} u\left(r,0\right) = \beta_1\tau_{rz}\left(r,0\right), v\left(r,0\right) = \beta_2\tau_{z\phi}\left(r,0\right) + r\omega, w = 0, \\ T\left(r,0\right) = T_w + \beta_3 T_z\left(r,0\right), \mathrm{C}\left(r,0\right) = C_w + \beta_4 C_z\left(r,0\right), \\ N\left(r,0\right) = N_w + \beta_5 N_z\left(r,0\right), u\left(r,0\right) \to 0, v\left(r,0\right) \to 0, \\ T\left(r,0\right) \to T_\infty, C\left(r,0\right) \to C_\infty, N\left(r,0\right) \to N_\infty \,\mathrm{as}\, z \to \infty \end{array}\right\} \tag{15}$$

where T stands for the temperature of nanofluid, C stands for the concentration of nanomaterials, N stands for the concentration of motile microorganisms, $\alpha_m = k/(\rho c)_f$ for thermal diffusivity, $(\rho c)_p$ for the heat capacity of nanomaterials, $(\rho c)_f$ for base fluid heat capacity, ρ signifies the fluid density, k for thermal conductivity, D_T for the coefficient of thermophoresis diffusion, D_B for Brownian diffusion coefficient, the term $16\sigma^* T_\infty^3/3k^*$ in Eq. (5) depicts the thermal radiative heat transfer. The term $Kr^2\left(C - C_\infty\right)\left(\frac{T}{T_\infty}\right)^n \exp\left(\frac{-E_a}{K_1 T}\right)$ in Eq. (6) represents the modified Arrhenius function where E_a denotes the activation energy and Kr is the chemical reaction rate, n power-law index, D_m the mass diffusion coefficient, W_c the maximum swimming speed of microorganism cell and β_1, β_2 are wall slip parameters.

The similarity transformations are [17,37]:

$$\begin{array}{l} \zeta = \left(\omega/v\right)^{\frac{1}{2}} z, \left(u, v, w\right) = \left(r\omega f'\left(\zeta\right), \mathrm{r}\omega g\left(\zeta\right), -2\sqrt{v\omega} f'\left(\zeta\right)\right), \\ \left(p, T, C, N\right) = \begin{pmatrix} p_\infty - \omega\mu P\left(\zeta\right), T_\infty + \left(T_w - T_\infty\right)\theta\left(\zeta\right), \\ C_\infty + \left(C_w - C_\infty\right)\phi\left(\zeta\right), N_\infty + \left(N_w - N_\infty\right)\chi\left(\zeta\right) \end{pmatrix} \end{array} \tag{16}$$

where $f\left(\zeta\right)$ and $g\left(\zeta\right)$ are the non-dimensional stream functions, $\theta\left(\zeta\right)$ is the non-dimensional temperature of nanofluid, $\phi\left(\zeta\right)$ is the non-dimensional nanoparticles concentration function, $\chi\left(\zeta\right)$ is the non-dimensional microorganisms density field, and ζ is the similarity transformation variable.

The following dimensionless ordinary differential equations are obtained by applying suitable similarity transformations [17,37]:

$$f''' - f'^2 + 2ff'' + g^2 + \lambda\left(f''^2 - 2f'f''' - g'^2\right) + B^*\left(\theta - Rb\phi - Rc\chi\right) = 0, \tag{17}$$

$$g'' - 2f'g + 2fg' - 2\lambda\left(f'g'' - f''g'\right) = 0, \tag{18}$$

$$\left(1 + \frac{4}{3}Rd\right)\theta'' + \Pr\left(f\theta' + Nb\theta'\phi' + Nt\theta'^2\right) = 0, \tag{19}$$

$$\phi'' + \frac{Nt}{Nb}\theta'' + LePrf\phi' - \Pr Le\sigma^* (1+\delta\theta)^n \exp(-E/(1+\delta\theta))\,\phi = 0, \tag{20}$$

$$\chi'' + Lbf\chi' - Pe\left[\phi''(\chi+\delta_1) + \chi'\phi'\right] = 0. \tag{21}$$

where the Reiner–Rivlin fluid parameter is $\lambda = \left(\frac{\mu_c\omega}{\mu}\right)$, $Rb = \left(\frac{\gamma(\rho_m-\rho_f)(N_w-N_\infty)}{\rho_f(1-C_\infty)(T_w-T_\infty)\beta^{**}}\right)$ and $Rc = \left(\frac{(\rho_p-\rho_f)(C_w-C_\infty)}{(T_w-T_\infty)\beta^{**}\rho_f(1-C_f)}\right)$ for bioconvection Rayleigh number as well as buoyancy ratio parameter, respectively, $Rd = 4\sigma T_\infty^3/kk^*$ thermal radiation parameter, $B^* = \left(\beta^{**}g^*\left(1-C_f\right)(T_w-T_\infty)(1-\gamma t)\right)/\omega r$ for mixed convection parameter, activation energy parameter read as $E = E_a/kT_\infty$, $Le = (\alpha_1/D_B)$ Lewis number, Prandtl number denoted by $\Pr = \left(\frac{\mu C_p}{k}\right)$, $Nb = \left(\frac{\tau D_B(C_W-C_\infty)}{\nu}\right)$ denotes Brownian diffusion parameter, $Nt = \left(\frac{\tau D_T(T_W-T_\infty)}{\nu T_\infty}\right)$ be the thermophoresis parameter, $Lb = \left(\frac{\nu}{D_m}\right)$, $Pe = \left(\frac{bW_c}{D_m}\right)$ and $\delta_1 = \left(\frac{N_\infty}{N_w-N_\infty}\right)$ for bioconvection Lewis number, Peclet number and microorganisms differences parameter, respectively.

Here $\gamma_1 = \left(\beta_3\sqrt{\nu/\omega}\right), \gamma_2 = \left(\beta_4\sqrt{\nu/\omega}\right)$ and $\gamma_3 = \left(\beta_5\sqrt{\nu/\omega}\right)$ for thermal, concentration and microorganisms slip coefficients where β_3, β_4 & β_5 are slip coefficients. Thus, the boundary conditions are transformed also [17,37]:

$$\left.\begin{array}{l} f(0)=0, f'(0)=\beta_1 f''(0)\left(1-2\lambda f'(0)\right), g(0)=\beta_2 g'(0)\left(1-2\lambda f'(0)\right)+1, \\ \theta(0)=1+\gamma_1\theta'(0), \phi(0)=1+\gamma_2\phi'(0), \chi(0)=1+\gamma_3\chi'(0) \\ f'\to 0, g\to 0, \theta\to 0, \phi\to 0, \chi\to 0 \; as\, \zeta\to\infty. \end{array}\right\} \tag{22}$$

Torque T_0 is specified by definite integral such as:

$$T_0 = -\int_0^R \tau_{z\phi}|_{z=0}\left(2\pi r^2\right)dr = -\frac{\pi\rho\omega}{2}\sqrt{\omega\nu}R^4 G'(0) \tag{23}$$

The engineering quantities of interest are local skin friction coefficient C_f (explain the shear stress on the surface), local Nusselt number Nu (explain the rate of heat transfer), Sherwood number Sh (explain the rate of mass transfer), as well as the local density number of motile microorganisms Sn (explain the motile microorganisms flux) are presented as:

$$C_f = \frac{\sqrt{\tau_r^2 - \tau_\phi^2}}{\rho(r\omega)^2},\ Nu = \frac{rq_w}{k(T_w-T_\infty)},\ Sh = \frac{rj_w}{D_B(C_w-C_\infty)},\ Sn = \frac{rj_m}{D_m(N_w-N_\infty)} \tag{24}$$

where q_w, j_w and j_m denotes shear stress, local heat flux, local mass flux, and motile microorganisms' flux on the surface, respectively.

$$q_w = -\left(k_f + \frac{16\sigma^* T_\infty^3}{3k^*}\right)\left(\frac{\partial T}{\partial z}\right)|_{z=0},\ j_w = -D_B\left(\frac{\partial C}{\partial z}\right)|_{z=0},\ j_m = -D_m\left(\frac{\partial N}{\partial z}\right)|_{z=0}.$$

Thus from (24), we have dimensionless quantities as:

$$C_f = \left(\frac{\omega r^2}{v}\right)^{-\frac{1}{2}} \sqrt{(F''(0))^2 - (G'(0))^2},\ Nu = \left(\frac{\omega r^2}{v}\right)^{\frac{1}{2}} \theta'(0),\ Sh = \left(\frac{\omega r^2}{v}\right)^{\frac{1}{2}} \phi'(0), \tag{25}$$
$$Sn = \left(\omega r^2/v\right)^{\frac{1}{2}} \chi'(0)$$

3 Numerical Scheme

The ordinary differential Eqs. (17)–(21) under the boundary conditions (22) are tackled by bvp4c method with the comfort of computing software MATLAB. The arrangement of non-linear governing ordinary differential equations (ODEs) is restructured to the initial-order ordinary differential equation (ODEs). Let

$$\begin{aligned} &f = q_1, f' = q_2, f'' = q_3, f''' = q_3', g = q_4, g' = q_5, \\ &g'' = q_5', \theta = q_6, \theta' = q_7, \theta'' = q_7', \phi = q_8, \phi' = q_9, \\ &\phi'' = q_9', \chi = q_{10}, \chi' = q_{11}, \chi'' = q_{11}' \end{aligned} \tag{26}$$

$$q_3' = \frac{q_2^2 - 2q_1q_3 - q_4^2 - \lambda\left(q_3^2 - q_5^2\right) - B^*\left(q_6 - Rbq_8 - Rcq_{10}\right)}{1 - 2\lambda q_2}, \tag{27}$$

$$q_5' = \frac{2q_2q_4 - 2q_1q_5 - 2\lambda q_3q_5}{1 - 2\lambda q_2}, \tag{28}$$

$$q_7' = \frac{-\Pr\left(q_1q_7 + Nbq_7q_9 + Ntq_7^2\right),}{\left(1 + \frac{4}{3}Rd\right)} \tag{29}$$

$$q_9' = -\frac{Nt}{Nb}q_7' - Le\Pr q_1q_9 + \Pr Le\sigma^*\left(1 + \delta q_6\right)^n \exp\left(\frac{-E}{(1 + \delta q_6)}\right) q_8, \tag{30}$$

$$q_{11}' = -Lbq_1q_{11} + Pe\left[q_9'\left(q_{10} + \delta_1\right) + q_{10}q_9\right] \tag{31}$$

with

$$\left.\begin{aligned} &q_1(0) = 0, q_2(0) = \beta_1 q_3(0)\left(1 - 2\lambda q_2(0)\right), q_4(0) = \beta_2 q_5(0)\left(1 - 2\lambda q_2(0)\right) + 1, \\ &q_6(0) = 1 + \gamma_1 q_7(0), q_8(0) = 1 + \gamma_2 q_9(0), q_{10}(0) = 1 + \gamma_3 q_{11}(0) \\ &q_2 \to 0, q_4 \to 0, q_6 \to 0, q_8 \to 0, q_{10} \to 0\ as\ \zeta \to \infty \end{aligned}\right\}. \tag{32}$$

4 Results and Discussion

The numerical solution of non-linear dimensionless ordinary differentiated structures (17)–(21) with boundary constraints given in expression (22) has been attained by the bvp4c function on MATLAB using a mathematical shooting scheme. The major focus of the current work is to observe the effect of several developing specific parameters against axial velocity $f(\zeta)$, radial velocity $f'(\zeta)$, azimuthal velocity $g(\zeta)$, the thermal field $\theta(\zeta)$ of nanomaterials, the concentration field $\phi(\zeta)$ of nanomaterials, and the motile microorganisms field $\chi(\zeta)$. The outcomes of dimensionless profiles are analyzed briefly with the aid of graphs and tabular data. Figs. 2–27 are delineated the effects of prominently involved parameters *vs.* flow fields.

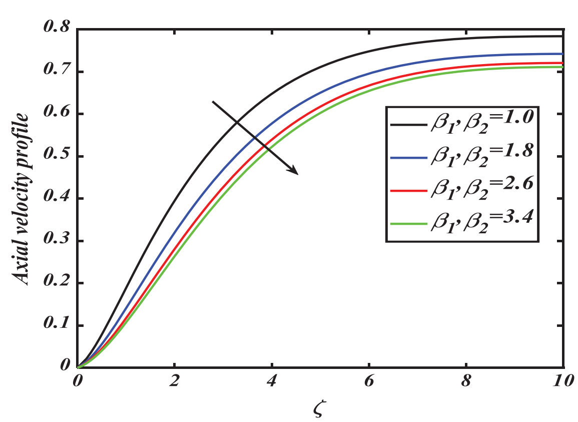

Figure 2: Axial velocity profile f for distinct values of wall slip parameters β_1, β_2

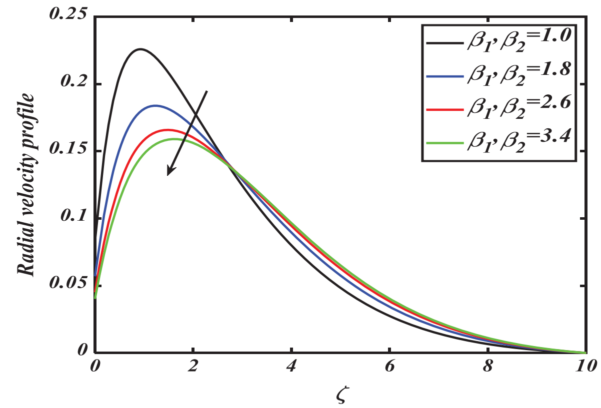

Figure 3: Radial velocity profile f' for distinct values of wall slip parameters β_1, β_2

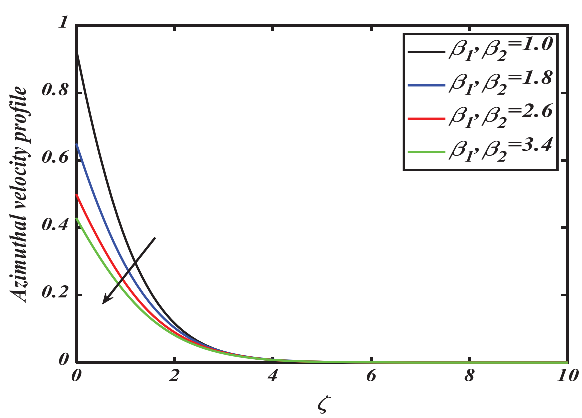

Figure 4: Azimuthal velocity profile g for distinct values of wall slip parameters β_1, β_2

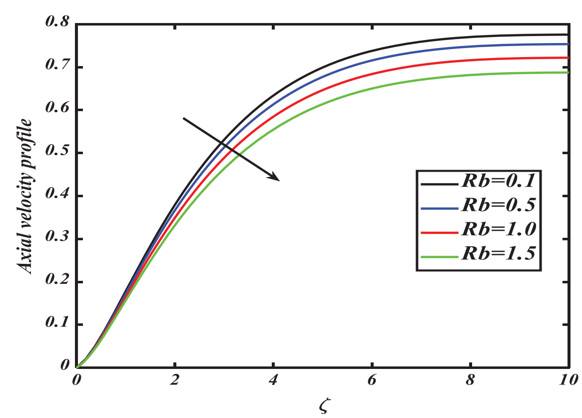

Figure 5: Axial velocity profile f for distinct values of bioconvection Rayleigh number Rb

Fig. 2 is depicted to see the impact of distinct estimations of wall slip parameters β_1, β_2 on the axial velocity profile f of Reiner–Rivlin nanofluid. It is manifest from the figure that increasing values of wall slip parameters diminishes the axial velocity profiles. Fig. 3 is designed to analyze the inspiration of wall slip parameters β_1, β_2 *vs.* radial fluid velocity f'. From the figure, it is also witnessed that radial fluid velocity decreases by enhancing the estimation of wall slip parameters. The significance of wall slips parameters β_1, β_2 on azimuthal velocity g is elaborated through Fig. 4. It is depicted that azimuthal velocity is depressed by enlarging wall slips parameters. Physically, wall slip occurs due to liquid-to-solid transitions under shear stress so crucially dependent on liquid-to-wall molecular interactions.

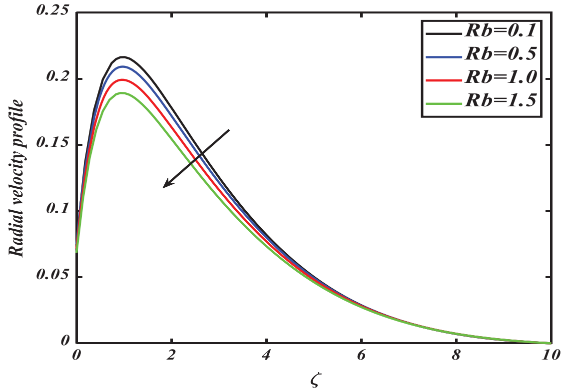

Figure 6: Radial velocity profile f' for distinct values of bioconvection Rayleigh number Rb

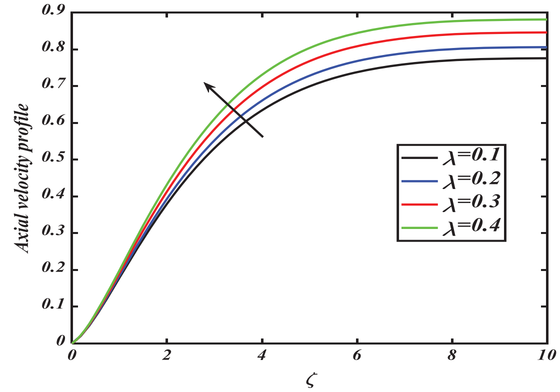

Figure 7: Axial velocity profile f for distinct values of Reiner–Revlin parameter λ

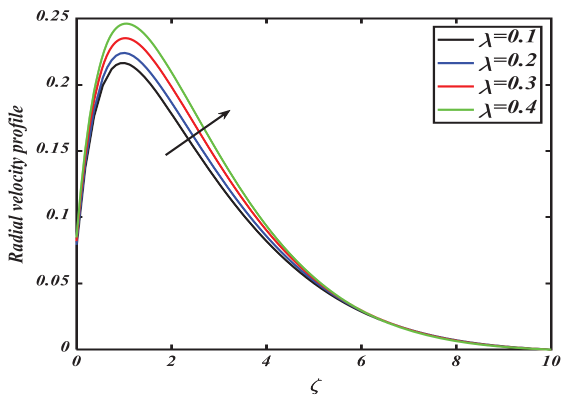

Figure 8: Radial velocity profile f' for distinct values of Reiner–Revlin parameter λ

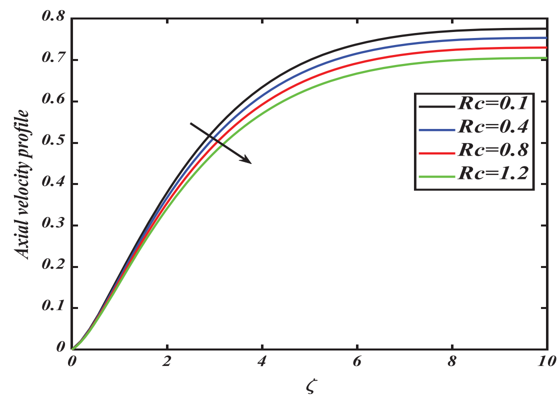

Figure 9: Axial velocity profile f for distinct values of buoyancy ratio parameter Rc

Figs. 5 and 6 demonstrate the inspiration of bioconvection Rayleigh number Rb against the axial and radial velocities f, f' of the fluid. It is observed that declination in velocities occurs with augmenting magnitudes of bioconvection Rayleigh number. Physically, the bioconvection Rayleigh number Rb measures the instability between layers of fluid due to the variation of temperature and density from top to bottom. The significance of the Reiner–Rivlin fluid parameter λ *vs.* axial and radial velocities f, f' are provided in Figs. 7 and 8. The rise in magnitudes of the Reiner–Rivlin fluid parameter λ diminishes both velocity fields of the fluid. Furthermore, radial velocity boosts up away from the disk. The variations of axial and radial velocities f, f' for distinct values of buoyancy ratio parameter Rc and mixed convection parameter B^* are presented in Figs. 9–12. The velocities escalate with higher magnitudes of mixed convection parameter while an opposing trend has been detected forbuoyancy ratio parameter. As mixed convection parameter exemplifies ratio among buoyancy to viscous force and large value of this parameter conveys higher buoyancy force, while buoyancy ratio develops further progressive for larger Rc which reduce velocities.

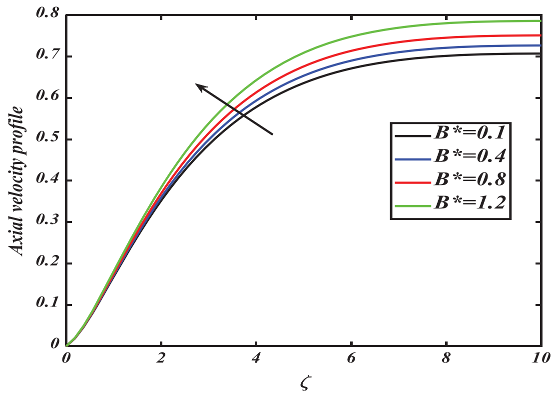

Figure 10: Axial velocity profile f for distinct values of mixed convection parameter B^{*}

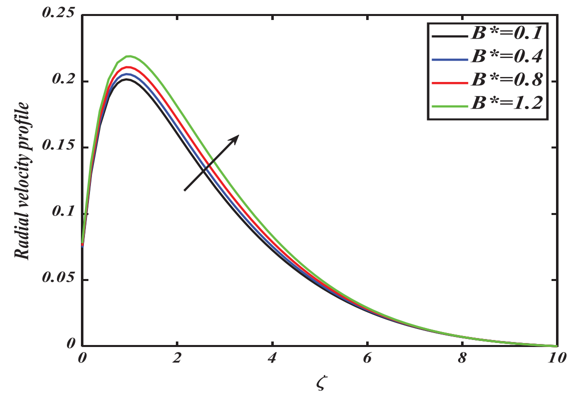

Figure 11: Radial velocity profile f' for distinct values of mixed convection parameter B^{*}

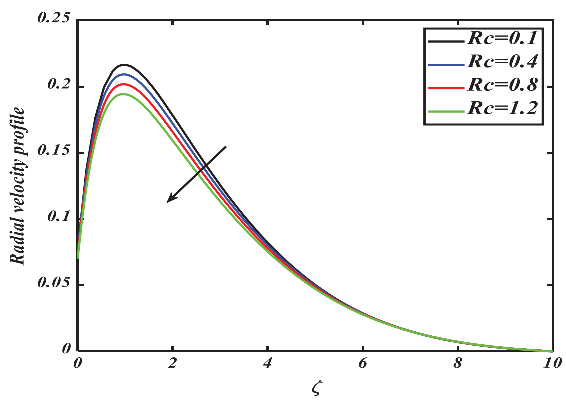

Figure 12: Radial velocity f' for distinct values of buoyancy ratio parameter Rc

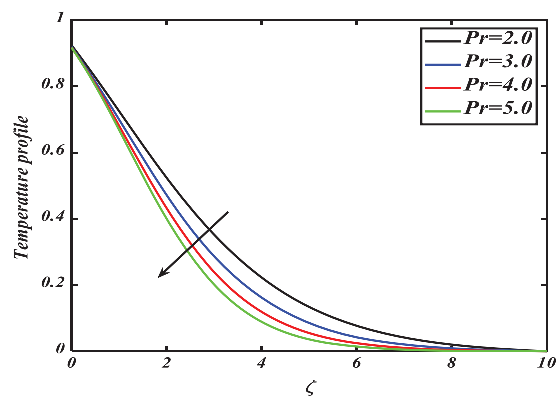

Figure 13: Temperature profile θ for distinct values of Prandtl number Pr

The dependence of temperature profile θ on relevant parameters is explained in Figs. 13–17. Fig. 13 demonstrates the outcomes of dimensionless temperature field θ against a varying range of Prandtl numbers Pr. Here, the temperature of nanofluid and its thermal boundary layer thickness declines for enlarging magnitudes of Prandtl number. Physically, when the Prandtl number boosted, the thermal diffusivity de-escalated and consequently led to the decrement in the ability of energy, so the thermal boundary layer declined. Fig. 14 discloses the stimulus of thermal slip coefficient γ_1 against a thermal field of species. The temperature field diminishes with rising numbers of thermal slip parameters. Fig. 15 is interpreted as the influence of distinct estimations of wall slip parameters β_1, β_2 on the temperature profile of Reiner–Rivlin nanofluid. It is apparent from the figure that emerging values of wall slip parameters β_1, β_2 boosted the concentration of the temperature field. The upshots of thermophoresis parameter Nt *vs.* temperature distribution θ are demonstrated in Fig. 16. Temperature distribution is increased by enlarging variation of thermophoresis parameter. Physically, this phenomenon occurs because the thermophoresis parameter raises the density of the thermal boundary layer, and suspended particles are transported from warmer to a cooler region which raises fluid temperature significantly. Therefore, temperature increases with an increase in Nt. Fig. 17 explaines the effects of thermal radiationRdon the thermal profile θ of nanofluids. The thermal field goes up due to augmentation in the values of the thermal radiation parameter. Physically, larger radiation parameter Rd leads to enhancement in the kinetic energy of fluid particles and hence increases the temperature profile of fluid.

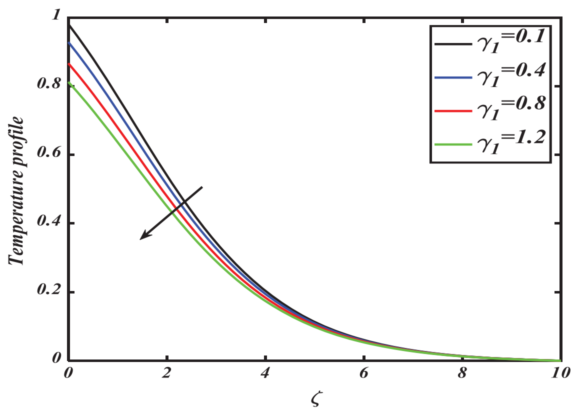

Figure 14: Temperature profile θ for distinct values of thermal slip coefficient γ_1

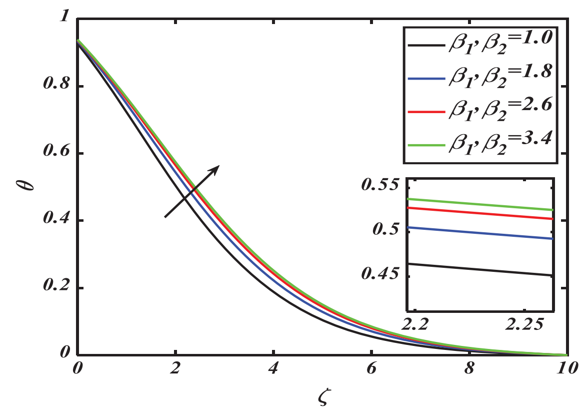

Figure 15: Temperature profile θ for distinct values of wall slip parameters β_1, β_2

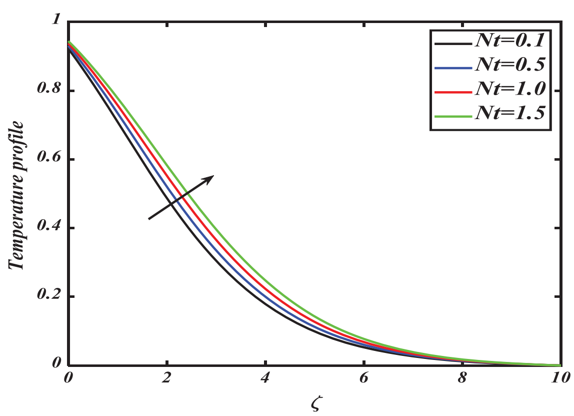

Figure 16: Temperature profile θ for distinct values of thermophoresis parameter Nt

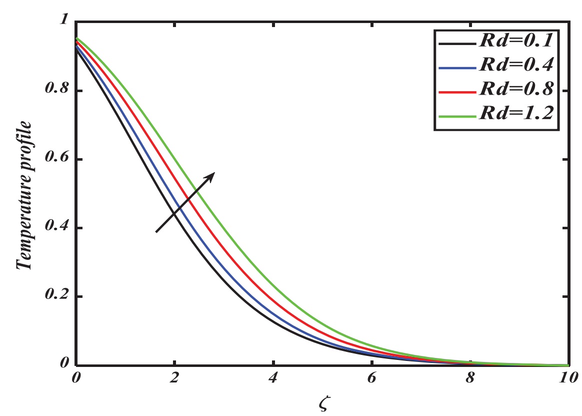

Figure 17: Temperature profile θ for distinct values of thermal radiation parameter Rd

Figs. 18–23 reveal a dependence of concentration distribution ϕ on the relevant parameters. Fig. 18 decelerates the consequence of the Brownian motion parameter Nb via the concentration profile ϕ of nanoparticles. It is inferred that the concentration of nanomaterials retarded down for larger estimations of the Brownian motion parameter. Physically, the greater Brownian motion results in an arbitrary movement of nanoparticles so the extra heat is produced. Due to this extra heat, the temperature of nanoparticles is also increased causes reduced nanoparticles concentration profile. Fig. 19 delineates the characteristics of Lewis number Le over concentration profile of species. Diminution in the concentration of Reiner–Rivlin nanofluid can be noticed for enlarging magnitudes of Lewis number. Physically, the Lewis number decreases the mass diffusivity and hence reduces the permeation depth of the boundary layer. Fig. 20 discloses the consequences of activation energy E against the volumetric concentration of nanoparticles. The volumetric concentration of nanoparticles is boosted by the intensification in the values of activation energy. Activation energy, the minimum energy required to start a chemical reaction. So, the volumetric concentration profile increases as E. The properties of the wall slip parameter on the solutal field of species are demonstrated in Fig. 21. Solutal profile decreases for larger magnitudes of concentration slip coefficient γ_2. Fig. 22 is deliberated to investigate the inspiration of wall slip parameters β_1, β_2 against the volumetric distribution of nanofluid. It is viewed that volumetric nanoparticle concentration enhancing parallel to the enlarging estimations of wall slip parameters β_1, β_2.

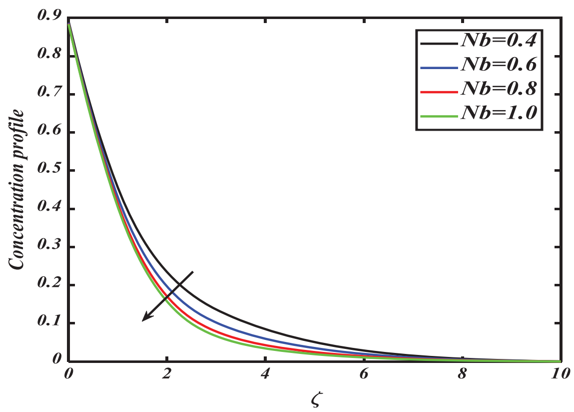

Figure 18: Nanoparticle concentration profile ϕ for distinct values of Brownian diffusion parameter Nb

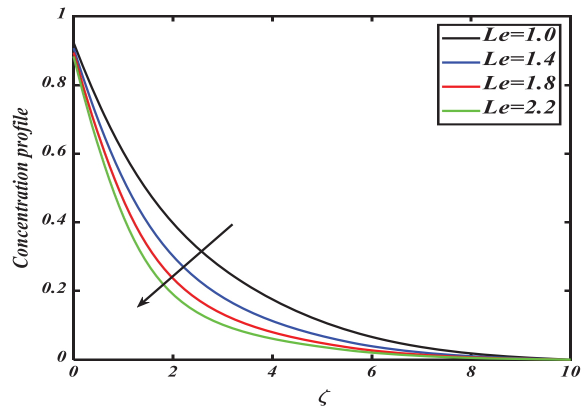

Figure 19: Nanoparticle concentration profile ϕ for distinct values of Lewis number Le

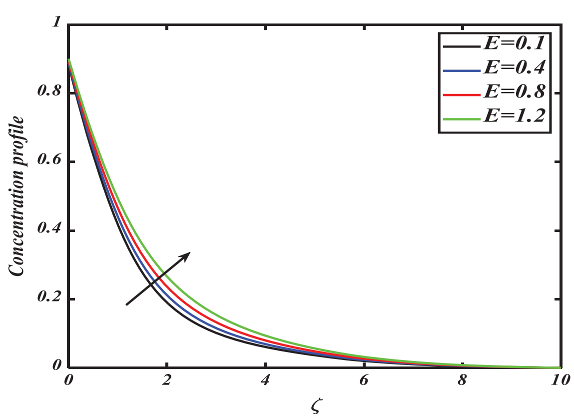

Figure 20: Nanoparticle concentration profile ϕ for distinct values of activation energy E

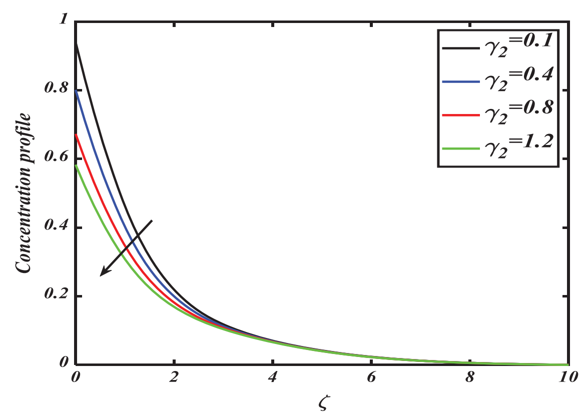

Figure 21: Nanoparticle concentration profile ϕ or distinct values of concentration slip coefficient γ_2

Fig. 23 is considered to study the upshot of thermophoresis parameter Nt on the solutal field ϕ of nanomaterials. It is observed that the thermophoresis parameter strongly enhanced the concentration field of species. Physically, in the thermophoresis phenomenon, the tiny particles of fluid are pulled back from the warm to a cold area. Then the particles of the nanofluid move back from the heated surface and consequently nanoparticles' volume profile is enhanced.

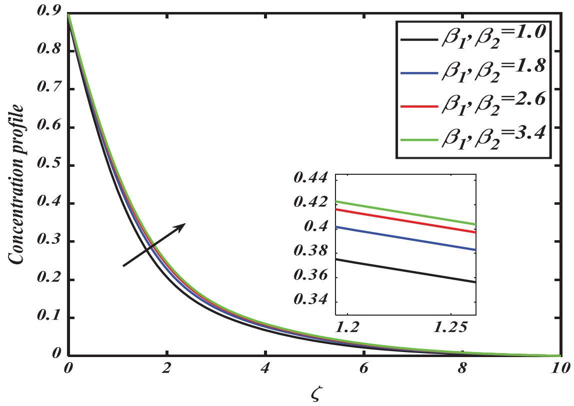

Figure 22: Nanoparticle concentration profile ϕ for distinct values of wall slip parameters β_1, β_2

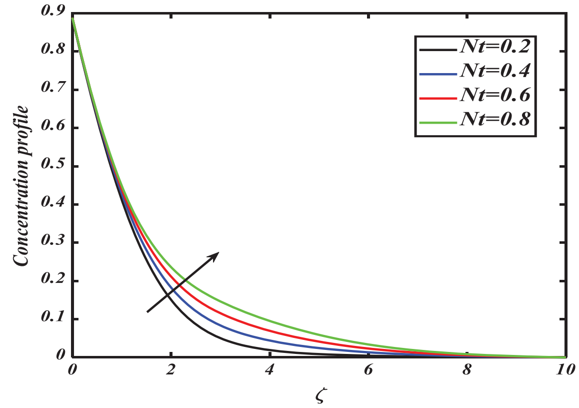

Figure 23: Nanoparticle concentration profile ϕ for distinct values of thermophoresis number Nt

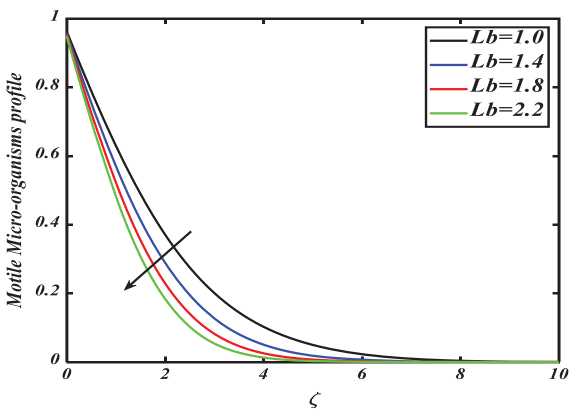

Figure 24: Motile microorganism density profile χ for distinct values of bioconvection Lewis number Lb

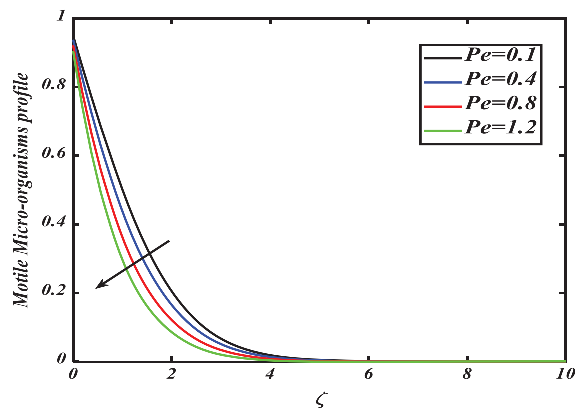

Figure 25: Motile microorganism density profile χ for distinct values of Peclet number Pe

Figs. 24–27 revealed the effectiveness of bioconvection Lewis number Lb, Peclet number Pe, microorganism slip coefficient γ_3, and wall slip parameters β_1, β_2 over the swimming motile microorganism's concentration field χ. Fig. 24 is plotted to allocate the influence of bioconvection Lewis number Lb over the swimming motile microorganism's concentration field χ. It is conceivable to note that the motile microorganisms' profile χ diminishes by positive variations of bioconvection Lewis number Lb. This happens, as the increasing values Lb increase the rate of viscous diffusion, and the density profile of motile microorganisms decreases in the boundary layer. Fig. 25 is drawn to outline the significance of bioconvection Peclet number Pe of motile gyrotactic microorganism's distribution χ. From the curves, it is promising to observe that the motile microorganisms' field χ reduces when the Peclet number boosts. As bioconvection Peclet number $Pe = \frac{bW_c}{D_m}$ increases, the cell swimming speed W_c also increases, and hence density profile of motile microorganisms decreases. Fig. 26 exhibits the variation of microorganism slip coefficient γ_3 against motile microorganism's distribution profile χ. From the graphs, it is perceived that the concentration of motile microorganism's profile curve declined for distinct estimations of microorganism slip coefficient. Fig. 27 reports the assortment of motile microorganisms' fields χ for evident estimations of wall slip parameters β_1, β_2. Enhancement in the wall slip parameters boosted the density of the motile microorganism's field.

Figs. 28a–28c show the streamlines at different values of the β_1, β_2. The contour of Nusselt number and Sherwood number against subjective parameters is shown in Figs. 29a and 29b. From the figures we observed that the Shewood number and Nusselt number are enhanced via larger subjective parameters. The 3-D plot of Nusslet number via *Rb* and *Rc* drawn in Fig. 30. Furthermore, the 3D plot of microorganism's density number for different estimations of the *Pe* and *Lb* given in Fig. 31.

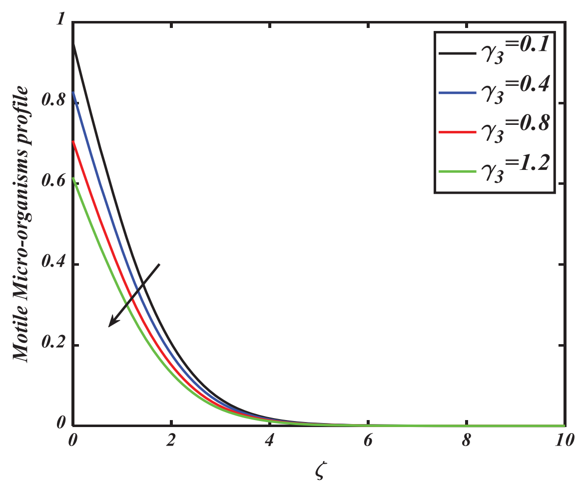

Figure 26: Motile microorganism density profile χ for distinct values of microorganisms slip coefficient γ_3

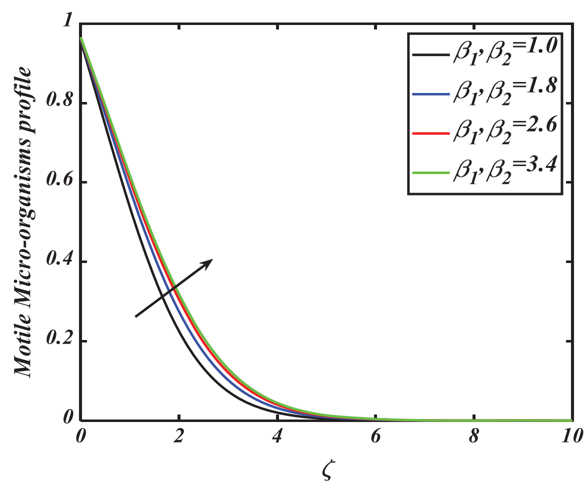

Figure 27: Motile microorganism density profile χ for distinct values of wall slip parameters β_1, β_2

Tables 1–3 are pinched to estimate the variations of the local Nusselt number, the local Sherwood number, as well as the local density number of swimming microorganisms against various mentioned parameters. From Table 1, it can be noted that the local Nusselt number (heat transfer rate) decreases through λ and Pr. Furthermore, the local Sherwood number (mass transfer rate) declined for larger magnitudes of the parameters *Rb* & *Rc*, and increases as γ_2 shown in Table 2. From Table 3, it is concluded that the local density number of microorganisms (motile microorganisms' flux) rises with *Pe* and *Lb*. Table 4 gives the comariosion of resuts between current study and results by Naqvi et al. [38].

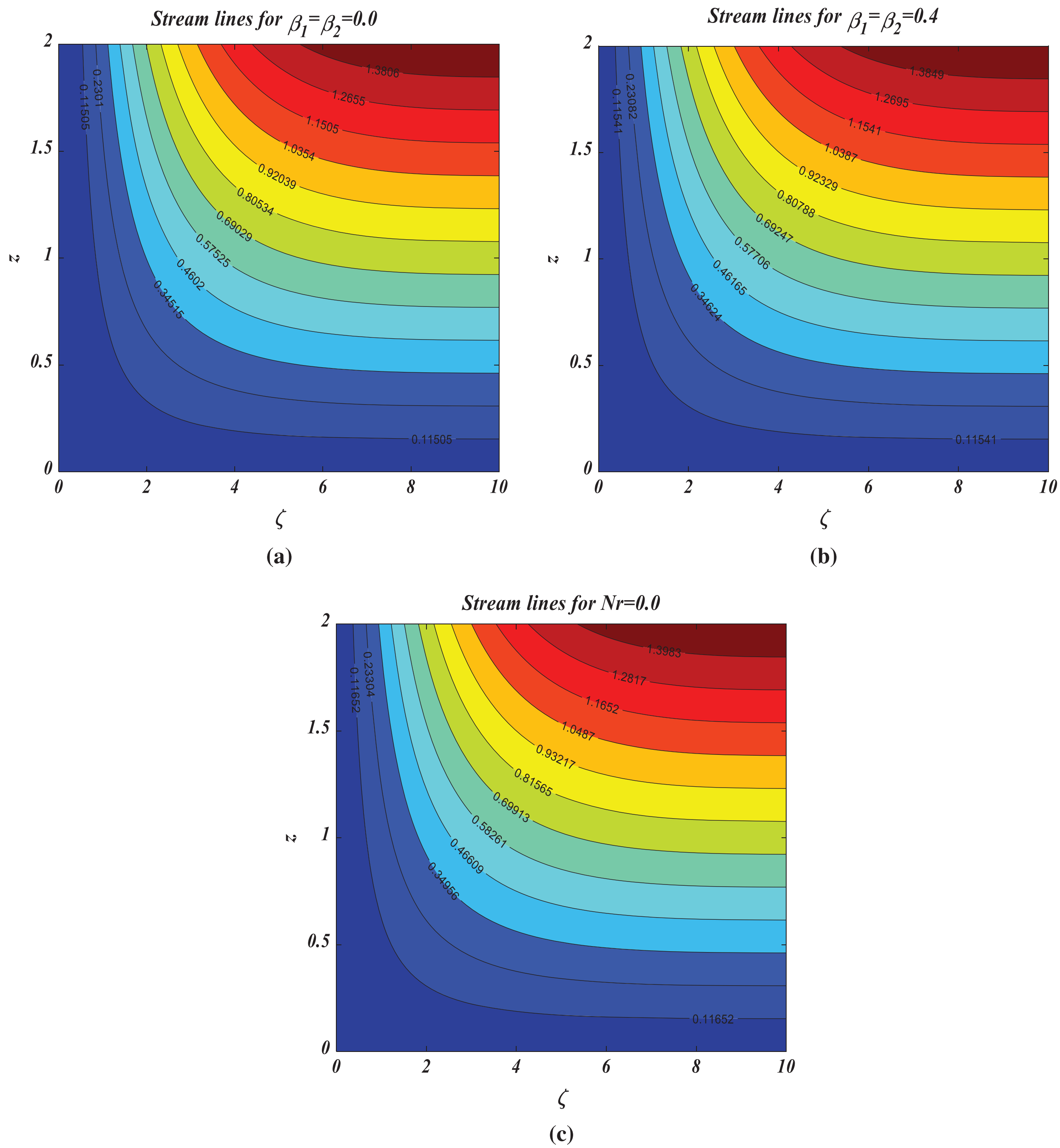

Figure 28: (a–c) Aspects of streamline Nr and $\beta_1 = \beta_2$

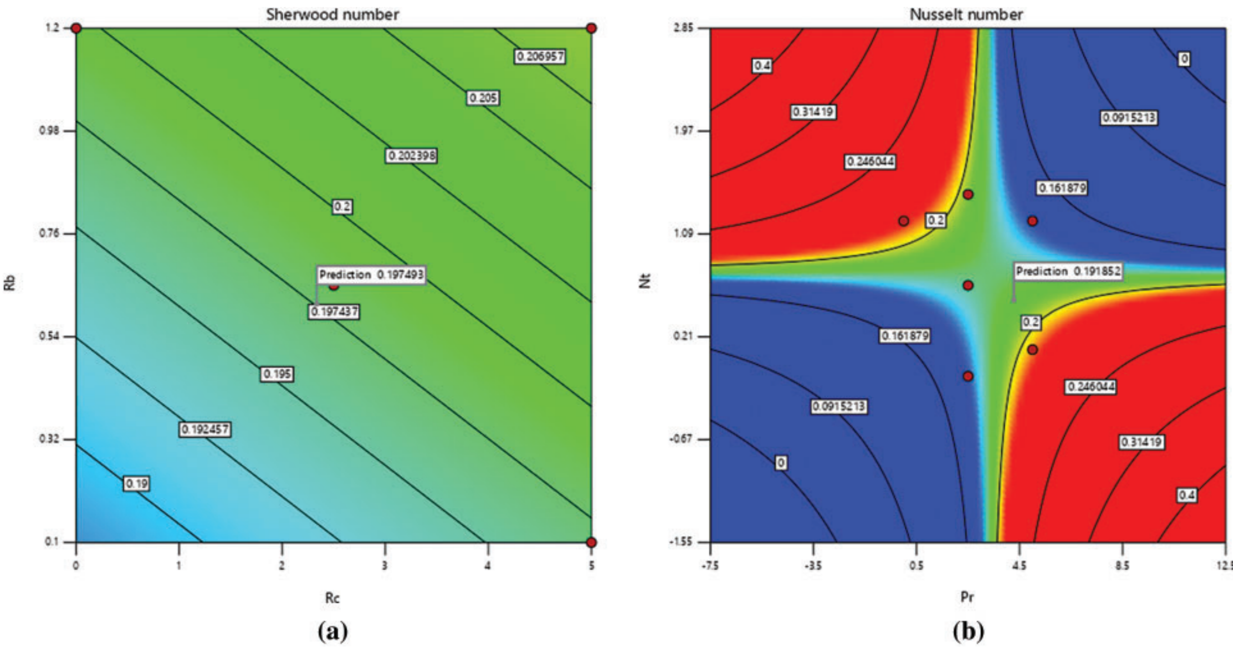

Figure 29: (a and b) Aspects of Contour line Sherwood and Nusselt number

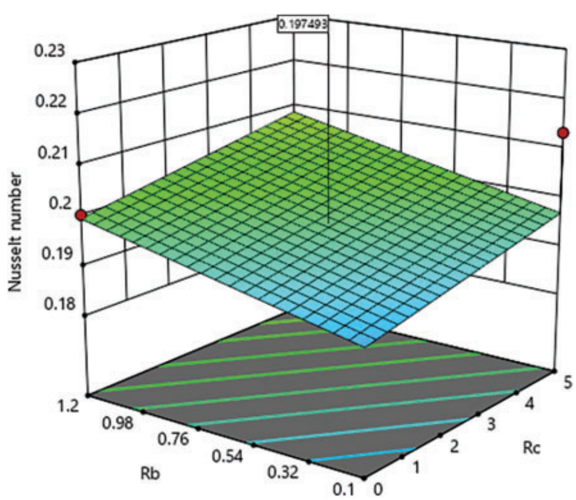

Figure 30: 3D plot of *Rb* & *Rc* on Nusselt number

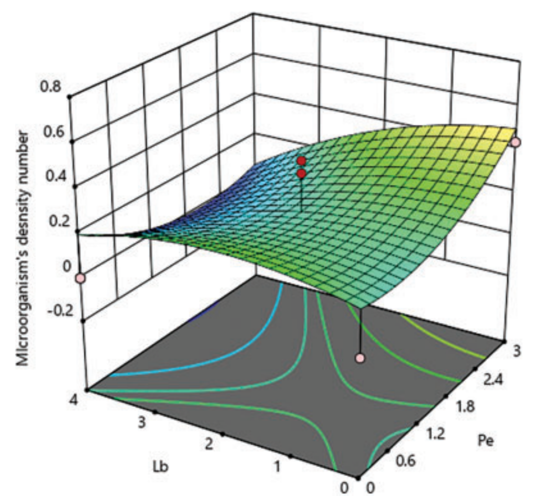

Figure 31: 3D plot of *Lb* & *Pe* on Microorganism's profile

Table 1: Tabulation of $-\theta'(0)$ with variations of Pr, λ, Nb, Nt, B^*, Rc, Rb and γ_1

Pr	Nb	Nt	λ	B^*	Rc	Rb	γ_1	$-\theta'(0)$
3.0	0.2	0.3	0.5	0.1	0.2	0.2	1.0	0.1772
4.0								0.1816
5.0								0.1832
1.2	0.1	0.3	0.5	0.1	0.2	0.2	1.0	0.2084
	0.6							0.2564
	1.2							0.2609
1.2	0.2	0.1	0.5	0.1	0.2	0.2	1.0	0.1996
		0.6						0.2043
		1.2						0.2089
	0.2	0.3	0.1	0.1	0.2	0.2	1.0	0.4064
			0.2					0.4156
			0.3					0.4245
1.2		0.3	0.5	0.2	0.2	0.2	1.0	0.1997
				0.3				0.2072
				0.4				0.2136
1.2	0.2	0.3	0.5	0.1	0.2	0.2	1.0	0.1930
					0.6			0.1867
					1.2			0.1809
1.2	0.2	0.3	0.5	0.1	0.2	0.2	1.0	0.2256
						0.6		0.2133
						1.2		0.2003
1.2	0.2	0.3	0.5		0.2	0.2	0.1	0.1701
				0.1			0.6	0.1801
							1.2	0.1874

Table 2: Tabulation of $-\phi'(0)$ with variations of Pr, Nb, Nt, λ, B^*, Rc, Rb, Le and γ_2

Pr	Nb	Nt	λ	B^*	Rc	Rb	Le	γ_2	$-\phi'(0)$
3.0	0.2	0.3	0.5	0.1	0.2	0.2	2.0	1.5	0.4574
4.0									0.5331
5.0									0.5972
1.2	0.1	0.3	0.5	0.1	0.2	0.2	2.0		0.3281
	0.6							1.5	0.3145
	1.2								0.3076
1.2	0.2	0.1	0.5	0.1	0.2	0.2	2.0	1.5	0.5070
		0.6							0.5090
		1.2							0.5113

(Continued)

Table 2: (continued)

Pr	Nb	Nt	λ	B^*	Rc	Rb	Le	γ_2	$-\phi'(0)$
	0.2	0.3	0.1	0.1	0.2	0.2	2.0	1.5	0.1924
			0.2						0.1910
			0.3						0.1894
1.2		0.3	0.5	0.2	0.2	0.2	2.0	1.5	0.3503
				0.3				1.5	0.3536
				0.4					0.3567
1.2	0.2	0.3	0.5	0.1	0.2	0.2		1.5	0.3473
					0.6				0.3404
					1.2				0.3359
1.2	0.2	0.3	0.5	0.1	0.2	0.2	2.0	1.5	0.2445
						0.6			0.2425
						1.2			0.2287
1.2	0.2	0.3	0.5	0.1	0.2	0.2	1.0	1.5	0.3462
							1.6		0.4464
							2.2		0.5193
1.2	0.2	0.3	0.5	0.1	0.2	0.2	2.0	0.2	0.3461
								1.0	0.3463
								3.0	0.3466

Table 3: Tabulation of $-\chi'(0)$ with variations of λ, B^*, Rc, Rb, Pe, Lb and γ_3

λ	B^*	Rc	Rb	Pe	Lb	γ_3	$-\chi'(0)$
0.1	0.1	0.2	0.2	0.1	2.0	0.3	0.3128
0.2							0.3108
0.3							0.3085
0.5	0.2	0.2	0.2	0.1	2.0	0.3	0.4263
	0.4						0.4323
	0.8						0.4394
0.5	0.1	0.2	0.2	0.1	2.0	0.3	0.4155
		0.6					0.4208
		1.2					0.4289
0.5	0.1		0.2	0.1	2.0	0.3	0.2425
			0.6				0.2353
			1.2				0.2313
0.5	0.1	0.2		0.2	2.0	0.3	0.4386
				0.6			0.5161
				1.2			0.6262
0.5	0.1	0.2	0.2	0.1	1.2	0.3	0.3370
					1.6		0.3815
					1.2		0.4353
0.5	0.1	0.2	0.2	0.1	2.0	0.1	0.3605
						0.6	0.3486
						1.2	0.3402

Table 4: Validations of β_1, β_2 and K

Parameters			Naqvi et al. [38]	Current result
β_1	β_2	K	$\sqrt{f''(0)^2 + g'(0)^2}$	$\sqrt{f''(0)^2 + g'(0)^2}$
1	2	1	0.306957	0.306957
1.5	2	1	0.313802	0.313802
2	2	1	0.319288	0.319288
2	2	1	0.319288	0.319288
2	3	1	0.240918	0.240918
2	4	1	0.193365	0.193365
2	2	0.2	0.425177	0.425177
2	2	0.7	0.309290	0.309290
2	2	1	0.319288	0.319288

5 Conclusions

In this manuscript, we have discussed the steady and incompressible bioconvection flow of Reiner–Rivlin nanofluid over a rough rotational disk containing motile microorganisms with thermal radiation and Arrhenius activation energy. The effects of some asymmetrical controlling parameters including wall slip parameters, thermophoresis parameter, Brownian motion parameter, Reiner–Revlin nanofluid parameter, Prandtl number, Peclet number, Lewis number, bioconvection Lewis number, and the mixed convection parameter on the flow, the concentration of nanoparticles, thermal field, and density of motile microorganisms are examined thoroughly.

- The velocity profiles of nanofluid escalate for higher magnitudes of mixed convection parameter B^* while an opposing trend has been detected for buoyancy ratio parameter Rc, Reiner–Rivlin fluid parameter λ, wall slip parameters β_1 & β_2, and bioconvection Rayleigh number Rb.
- The temperature profile of nanofluid goes up due to augmentation in the values of thermal radiation parameter Rd, thermophoresis number Nt, and wall slip parameters β_1 & β_2 while an opposing trend has been noticed for enlarging magnitudes of Prandtl number Pr.
- The concentration profile is boosted up by the thermophoresis number Nt and wall slip parameters β_1 & β_2.
- The concentration profile of nanoparticles grows by intensification in activation energy E.
- Brownian motion Nb and Lewis number Le consequences show a decrement in the concentration profile of nanoparticles.
- The motile microorganisms' profile diminishes by positive variations of bioconvection Lewis number Lb and Peclet number Pe while escalating for wall slip parameters β_1 & β_2.
- The temperature, concentration, and microorganisms' density profiles decrease for enlarging values of thermal, concentration, and microorganisms slip coefficients γ_1, γ_2 & γ_3, respectively.

Funding Statement: This work is financially supported by the Government College University, Faisalabad, and Higher Education Commission, Pakistan.

Conflicts of Interest: The authors declare that they have no conflicts of interest to report regarding the present study.

References

1. Choi, S. U., Eastman, J. A. (1995). *Enhancing the thermal conductivity of fluids with nanoparticles*(No. AL/MSD/CP-84938; CONF-951135-29). IL, USA: Argonne National Lab.
2. Buongiorno, J. (2005). Convective transport in nanofluids. *ASME Journal of Heat Transfer, 128(3),* 240–250. DOI 10.1115/1.2150834.
3. Sheikholeslami, M., Bhatti, M. M. (2017). Forced convection of nanofluid in presence of constant magnetic field considering shape effects of nanoparticles. *International Journal of Heat and Mass Transfer, 111(7),* 1039–1049. DOI 10.1016/j.ijheatmasstransfer.2017.04.070.
4. Waqas, H., Farooq, U., Naseem, R., Hussain, S., Alghamdi, M. (2021). Impact of MHD radiative flow of hybrid nanofluid over a rotating disk. *Case Studies in Thermal Engineering, 26(1),* 101015. DOI 10.1016/j.csite.2021.101015.
5. Bhatti, M. M., Rashidi, M. M. (2016). Effects of thermo-diffusion and thermal radiation on Williamson nanofluid over a porous shrinking/stretching sheet. *Journal of Molecular Liquids, 221(4),* 567–573. DOI 10.1016/j.molliq.2016.05.049.
6. Hafeez, A., Khan, M., Ahmed, J. (2020). Stagnation point flow of radiative Oldroyd-B nanofluid over a rotating disk. *Computer Methods and Programs in Biomedicine, 191(17),* 105342. DOI 10.1016/j.cmpb.2020.105342.
7. Hayat, T., Imtiaz, M., Alsaedi, A. (2015). MHD 3D flow of a nanofluid in the presence of convective conditions. *Journal of Molecular Liquids, 212(5),* 203–208. DOI 10.1016/j.molliq.2015.09.012.
8. Ellahi, R., Hussain, F., Abbas, S. A., Sarafraz, M. M., Goodarzi, M. et al. (2020). Study of two-phase Newtonian nanofluid flow hybrid with Hafnium particles under the effects of slip. *Inventions, 5(1),* 6. DOI 10.3390/inventions5010006.
9. Alsaedi, A., Hayat, T., Qayyum, S., Yaqoob, R. (2020). Eyring-Powell nanofluid flow with nonlinear mixed convection: Entropy generation minimization. *Computer Methods and Programs in Biomedicine, 186(3),* 105183. DOI 10.1016/j.cmpb.2019.105183.
10. Khan, M., Salahuddin, T., Tanveer, A., Malik, M. Y., Hussain, A. (2019). Change in internal energy of thermal diffusion stagnation point Maxwell nanofluid flow along with solar radiation and thermal conductivity. *Chinese Journal of Chemical Engineering, 27(10),* 2352–2358. DOI 10.1016/j.cjche.2018.12.023.
11. Gireesha, B. J., Krishnamurthy, M. R., Ganeshkumar, K. (2019). Nonlinear radiative heat transfer and boundary layer flow of Maxwell nanofluid past stretching sheet. *Journal of Nanofluids, 8(5),* 1093–1102. DOI 10.1166/jon.2019.1661.
12. Khan, M., Malik, M. Y., Salahuddin, T., Khan, F. (2019). Generalized diffusion effects on Maxwell nanofluid stagnation point flow over a stretchable sheet with slip conditions and chemical reaction. *Journal of the Brazilian Society of Mechanical Sciences and Engineering, 41(3),* 138. DOI 10.1007/s40430-019-1620-3.
13. Nadeem, S., Haq, R. U., Khan, Z. H. (2014). Numerical study of MHD boundary layer flow of a Maxwell fluid past a stretching sheet in the presence of nanoparticles. *Journal of the Taiwan Institute of Chemical Engineers, 45(1),* 121–126. DOI 10.1016/j.jtice.2013.04.006.
14. Khan, S. U., Tlili, I., Waqas, H., Imran, M. (2020). Effects of nonlinear thermal radiation and activation energy on modified second-grade nanofluid with Cattaneo–Christov expressions. *Journal of Thermal Analysis and Calorimetry, 143(2),* 1175–1186. DOI 10.1007/s10973-020-09392-6.
15. Alghamdi, M. (2020). On magnetohydrodynamic flow of viscoelastic nanofluids with homogeneous-heterogeneous reactions. *Coatings, 10(1),* 55. DOI 10.3390/coatings10010055.

16. Ullah, M. Z., Serra-Capizzano, S., Baleanu, D. (2020). A numerical simulation for Darcy–Forchheimer flow of nanofluid by a rotating disk with partial slip effects. *Frontiers in Physics, 7,* 219. DOI 10.3389/fphy.2019.00219.
17. Tabassum, M., Mustafa, M. (2018). Numerical treatment for partial slip flow and heat transfer of non-Newtonian Reiner–Rivlin fluid due to rotating disk. *International Journal of Heat and Mass Transfer, 123,* 979–987. DOI 10.1016/j.ijheatmasstransfer.2018.03.040.
18. Motsa, S., Makukula, Z. (2013). On spectral relaxation method approach for steady von Kármán flow of a Reiner–Rivlin fluid with Joule heating, viscous dissipation, and suction/injection. *Open Physics, 11(3),* 363–374. DOI 10.2478/s11534-013-0182-8.
19. Akbar, N. S., Nadeem, S. (2010). Simulation of heat and chemical reactions on Reiner–Rivlin fluid model for blood flow through a tapered artery with stenosis. *Heat and Mass Transfer, 46(5),* 531–539. DOI 10.1007/s00231-010-0595-5.
20. Baker, M., Ericksen, J. L. (1954). Inequalities restricting the form of the stress-deformation relations for isotropic elastic solids and Reiner–Rivlin fluids. *Journal of the Washington Academy of Sciences, 44(2),* 33–35.
21. Ansari, M. S., Otegbeye, O., Trivedi, M., Gogo, S. P. (2021). Magnetohydrodynamic bio-convective Casson nanofluid flow: A numerical simulation by paired quasi linearisation. *Journal of Applied and Computational Mechanics, 7(4),* 2024–2039. DOI 10.22055/JACM.2020.31205.1839.
22. Rashad, A. M., Nabwey, H. A. (2019). Gyrotactic mixed bioconvection flow of a nanofluid past a circular cylinder with convective boundary condition. *Journal of the Taiwan Institute of Chemical Engineers, 99(21),* 9–17. DOI 10.1016/j.jtice.2019.02.035.
23. Mamatha, S. U., Babu, K. R., Prasad, P. D., Raju, C. S. K., Varma, S. V. K. (2020). Mass transfer analysis of two-phase flow in a suspension of microorganisms. *Archives of Thermodynamics, 41,* 175–192. DOI 10.24425/ather.2020.132954.
24. Iqbal, Z., Mehmood, Z., Azhar, E., Maraj, E. N. (2017). Numerical investigation of nanofluid transport of gyrotactic microorganisms submerged in the water towards the Riga plate. *Journal of Molecular Liquids, 234,* 296–308. DOI 10.1016/j.molliq.2017.03.074.
25. Kasaragadda, S., Alarifi, I. M., Rahimi-Gorji, M., Asmatulu, R. (2020). Investigating the effects of surface superhydrophobicity on moisture ingression of nanofiber-reinforced bio-composite structures. *Microsystem Technologies, 26(2),* 447–459. DOI 10.1007/s00542-019-04507-y.
26. Waqas, H., Imran, M., Muhammad, T., Sait, S. M., Ellahi, R. (2021). On bio-convection thermal radiation in Darcy–Forchheimer flow of nanofluid with gyrotactic motile microorganism under Wu's slip over stretching cylinder/plate. *International Journal of Numerical Methods for Heat & Fluid Flow, 31(5),* 1520–1546. DOI 10.1108/HFF-05-2020-0313.
27. Amirsom, N. A., Uddin, M. J., Basir, M. F. M., Ismail, A., Beg, O. A. et al. (2019). Three-dimensional bioconvection nanofluid flow from a biaxial stretching sheet with anisotropic slip. *Sains Malaysiana, 48(5),* 1137–1149. DOI 10.17576/jsm-2019-4805-23.
28. Uddin, M. J., Kabir, M. N., Alginahi, Y., Bég, O. A. (2019). Numerical solution of bio-nano-convection transport from a horizontal plate with blowing and multiple slip effects. *Proceedings of the Institution of Mechanical Engineers, Part C: Journal of Mechanical Engineering Science, 233(19–20),* 6910–6927. DOI 10.1177/0954406219867985.
29. Ferdows, M., Reddy, M. G., Alzahrani, F., Sun, S. (2019). Heat and mass transfer in a viscous nanofluid containing a gyrotactic micro-organism over a stretching cylinder. *Symmetry, 11(9),* 1131. DOI 10.3390/sym11091131.
30. Khan, N. S., Shah, Q., Bhaumik, A., Kumam, P., Thounthong, P. et al. (2020). Entropy generation in bioconvection nanofluid flow between two stretchable rotating disks. *Scientific Reports, 10(1),* 4448. DOI 10.1038/s41598-020-61172-2.
31. Li, Y., Waqas, H., Imran, M., Farooq, U., Mallawi, F. et al. (2020). A numerical exploration of modified second-grade nanofluid with motile microorganisms, thermal radiation, and Wu's slip. *Symmetry, 12(3),* 393. DOI 10.3390/sym12030393.

32. Muhammad, T., Alamri, S. Z., Waqas, H., Habib, D., Ellahi, R. (2020). Bioconvection flow of magnetized Carreau nanofluid under the influence of slip over a wedge with motile microorganisms. *Journal of Thermal Analysis and Calorimetry, 143(2),* 945–957. DOI 10.1007/s10973-020-09580-4.
33. Song, Y. Q., Waqas, H., Al-Khaled, K., Farooq, U., Khan, S. U. et al. (2021). Bioconvection analysis for Sutter by nanofluid over an axially stretched cylinder with melting heat transfer and variable thermal features: A Marangoni and solutal model. *Alexandria Engineering Journal, 60(5),* 4663–4675. DOI 10.1016/j.aej.2021.03.056.
34. Al-Mubaddel, F. S., Farooq, U., Al-Khaled, K., Hussain, S., Khan, S. U. et al. (2021). Double stratified analysis for bioconvection radiative flow of Sisko nanofluid with generalized heat/mass fluxes. *Physica Scripta, 96(5),* 055004. DOI 10.1088/1402-4896/abeba2.
35. Farooq, U., Waqas, H., Khan, M. I., Khan, S. U., Chu, Y. M. et al. (2021). Thermally radioactive bioconvection flow of Carreau nanofluid with modified Cattaneo–Christov expressions and exponential space-based heat source. *Alexandria Engineering Journal, 60(3),* 3073–3086. DOI 10.1016/j.aej.2021.01.050.
36. Zhang, T., Khan, S. U., Imran, M., Tlili, I., Waqas, H. et al. (2020). Activation energy and thermal radiation aspects in bioconvection flow of rate type nanoparticles configured by a stretching/shrinking disk. *Journal of Energy Resources Technology, 142(11),* 112102. DOI 10.1115/1.4047249.
37. Waqas, H., Imran, M., Muhammad, T., Sait, S. M., Ellahi, R. (2021). Numerical investigation on bioconvection flow of Oldroyd-B nanofluid with nonlinear thermal radiation and motile microorganisms over a rotating disk. *Journal of Thermal Analysis and Calorimetry, 145(2),* 523–539. DOI 10.1007/s10973-020-09728-2.
38. Naqvi, S. M. R. S., Kim, H. M., Muhammad, T., Mallawi, F., Ullah, M. Z. (2020). Numerical study for slip flow of Reiner–Rivlin nanofluid due to a rotating disk. *International Communications in Heat and Mass Transfer, 116(6),* 104643. DOI 10.1016/j.icheatmasstransfer.2020.104643.